Hindawi
Adsorption Science & Technology
Volume 2023, Article ID 2724122, 14 pages
https://doi.org/10.1155/2023/2724122

Review Article

Partial Purification of Anthocyanins (*Brassica oleracea* var. Rubra) from Purple Cabbage Using Natural and Modified Clays as Adsorbent

Darlyson Tavares Guimarães,[1,2] Liana Maria Ramos Mendes,[1,2] Luiz Bruno de Sousa Sabino,[1] Edy Sousa de Brito,[2] Enrique Vilarrasa-García,[1] Enrique Rodríguez-Castellón,[3] Juan Antonio Cecilia,[3] and Ivanildo José da Silva Junior[1]

[1]*Department of Chemical Engineering, Universidade Federal do Ceará, Av. Mister Hull, 2977, Campus Universitário do Pici, Fortaleza, Ceará 60356-000, Brazil*
[2]*Embrapa Tropical Agroindustry, R. Dra Sara Mesquita, 2270, Fortaleza, Ceará 60511-110, Brazil*
[3]*Department of Inorganic Chemistry, Crystallography and Mineralogy, Faculty of Sciences, Universidad de Málaga, Campus of Teatinos, 29071 Málaga, Spain*

Correspondence should be addressed to Juan Antonio Cecilia; jacecilia@uma.es

Received 16 January 2023; Revised 2 August 2023; Accepted 29 November 2023; Published 13 December 2023

Academic Editor: Senthil Kumar Ponnusamy

This research is aimed at evaluating strategies for the adsorption and recovery of anthocyanins present in purple cabbage using natural and modified clays as adsorbent. In the batch adsorption experiments, the anthocyanin extracts were put in contact with the adsorbents, and different parameters were evaluated to determine the best conditions for their adsorption and recovery. It was noted that the highest levels of adsorption (28.0 mg g^{-1}) occurred using a porous clay heterostructure (PCH) material as adsorbent, with a mass of 25 mg and 120 min of contact. Under the same conditions, the sepiolite only presented an adsorption capacity of 14.0 mg g^{-1}. The desorption results showed that the 60% methanolic solution recovered 60% of the anthocyanins adsorbed on PCH, while the 80% ethanolic solution recovered 35% of those adsorbed on sepiolite. The eluted anthocyanin solutions showed a 98% lower sugar concentration than the crude extract, indicating the low affinity of the adsorbents for sugars. Six types of acylated cyanidins were identified via UPLC-QToF-MSE in the extract, and it was confirmed from the FTIR analyses that the highest affinity of the clays occurred with the anthocyanins that presented more organic acid in their structure. The results show that PCH and sepiolite have high selectivity for anthocyanins and low affinity for the sugars present in the plant extract, facilitating the process of partial purification and application of these pigments.

1. Introduction

Anthocyanins (ACNs) are flavonoids widely distributed in nature, being responsible for the color of different flowers, fruits, and leaves, and also acting to protect the plant. Due to their variety of colors and recognized biological actions (e.g., antioxidant, anticancer, and anti-inflammatory actions), there is scientific interest in applying ACNs in several biomedical and technological applications [1]. Nowadays, the industrial applications of ACNs are limited, basically, by two factors. The absence of available and cheap substrates for their extraction and their marked instability to processing conditions, such as light, oxygen, and high temperatures, which can result in a loss of color. As a potential alternative, acylated ACNs are known to be a class of these pigments that display natural stability, presenting interesting potential for the industry. In this research, purple cabbage (*Brassica oleracea* var. Rubra) was used as a substrate for

the extraction of ACNs, which, beyond being an available and cheap raw material, presents in its constitution different types of acylated ACNs [2].

Depending on the application, purified ACN extracts are required, since the presence of coextracted substances, such as sugars and organic acids, can lead to pigment degradation [3]. Several techniques have been used to obtain purified ACNs. Thus, purification methods range from simple alternatives, such as solid-phase extraction (SPE) and liquid-liquid extraction, to the use of more sophisticated chromatographic techniques, such as countercurrent chromatography (CCC) and medium pressure liquid chromatography [4]. Generally, these methods exhibited unsatisfactory performance or make the process more complex and expensive. Adsorption is a widely used separation method due to its simplicity and economic viability [5].

To achieve a sustainable and competitive process, it is necessary to search for and develop materials that attain a good adsorption capacity and, in turn, are economically viable. Focusing on the ACN adsorption, synthetic and natural adsorbents such as ion-exchange resins [6, 7], commercial clay Tonsil Terrana 580FF [5, 8], and coal obtained from the Pequi bark [9] were previously reported for the purification of ACNs. Among them, natural clays can be highlighted due to their high availability on the earth's surface, low cost, and high versatility to modify their physicochemical properties, improving adsorption capacity [10, 11].

Among the raw clays, fibrous clays such as attapulgite (ATA) or sepiolite (SEP) have been extensively studied in adsorption processes due to their interesting fibrous morphology with high microporosity in their fibers because of the inversion of the tetrahedral sheet of the clay [12]. This results in a material with low density and high specific surface area [12–14]. Smectites are other phyllosilicates of great interest to the scientific community due to the charge deficiency of these phyllosilicates in their sheets, which must be counterbalanced with the presence of cations in the interlayer space. This fact encourages that smectites show a good trend in exchanging cations located in the interlayer space as well as hosting other cations or organic molecules in their interlaminar space, in such a way that make these phyllosilicates of great interest in the field of adsorption [11, 12]. The ability to exchange interlayer spaced alkaline or alkaline-earth cations by bulkier cations, as substitute bulkier cations in the interlayer space, promotes the incorporation of bulky polyoxocations or organic cations, which can be used to form pillared clays, improving textural properties of the clays substantially [11, 15].

Among the possible pillared clays, porous clay heterostructures (PCHs) have emerged as interesting materials for adsorption and catalytic processes [11, 16–19]. PCH synthesis was first described by Galarneau et al. in 1995 [16]. In this synthesis, a smectite is treated with a bulky organic cation solution to expand the interlayer space. After removing the nonintercalated organic cation, a silicon alkoxide is added to the mother solution, which polymerizes around the cation between adjacent sheets. Finally, the obtained gel is calcined to remove the organic cation, obtaining a porous material, which displays great porosity and high thermal stability, as well as high potential in the fields of adsorption and catalysis [11, 17].

Considering the importance of obtaining purified ACN extracts for their application as antioxidant, anticancer, or anti-inflammatory actions, through a simple and less expensive process such as adsorption, this study is aimed at evaluating the best conditions for the purification of ACNs extracted from purple cabbage using inexpensive adsorbents, such as natural and modified clays. The originality of this work lies in the study of several clay minerals in the present research that have not yet been evaluated in adsorption processes of ACNs. In addition, the study of PCHs in ACN purification processes has not been evaluated either. On the other hand, this manuscript is not limited to carrying out adsorption studies, since another goal of this study is the desorption of ACNs for subsequent valorization, as well as the quantification of adsorbed sugars and the possible determination of the ACN adsorbent.

2. Materials and Methods

2.1. Chemical Reagents. Ethanol (96 vol.%), acetone, methanol, and trifluoracetic acid were obtained from Sigma-Aldrich (Saint Louis, USA), HPLC grade. Acetonitrile and methanol from J.T.Baker (Pennsylvania, USA) were reagent grade, while the purity of H_2O was Milli-Q grade (Millipore Lab., Bedford, MA).

The natural fibrous clays (sepiolite and attapulgite) were provided by TOLSA. Bentonite was obtained from La Serrata de Níjar deposits located in the southeast of Spain [20]. PCH was synthesized from the bentonite sample [21].

2.2. Synthesis of the Porous Clay Heterostructures. The porous clay heterostructures (PCHs) were synthesized following the methodology described by Cecilia et al. with some modifications [11, 21]. 2.5 g of bentonite remained under stirring with 1 M NaCl solution for 1 day. Then, the homoionic bentonite underwent a cationic exchange with an excess bulky cation (9 g of cetyltrimethylammonium bromide in 100 mL of 1-propanol for 3 days). In the next step, the expanded bentonite was filtered and washed with H_2O to remove the excess cetyltrimethylammonium bromide, and then, the sample was resuspended in 250 mL of H_2O for 1 day. After that, 0.9 g of hexadecylamine was dissolved in 25 mL of 1-propanol and added dropwise into the mother solution, maintaining the stirring for 1 day. After this time, a solution of 12 mL of tetraethyl orthosilicate (TEOS), as a silicon source, dissolved in 12 mL of 1-propanol was added dropwise into the mother solution, maintaining this stirring for 3 days. Then, the gel was filtered and washed, and finally, the solid was dried at 80°C overnight and calcined at 550°C for 6 h to remove the organic template, forming a porous structure.

2.3. Characterization Techniques. X-ray powder diffraction (XRD) patterns have been performed on an automated X'Pert Pro MPD diffractometer (Malvern Panalytical, United Kingdom) with a primary monochromator Ge (111) (strictly monochromatic Cu Kα1 radiation) and an X'Celerator (real-time multiple strip) detector. The powder

profiles were recorded between 2° and 70° in 2θ with a total measuring time of 30 min and at a scanning rate of 2°/min.

The morphology of the clays was determined by Transmission Electron Microscopy (TEM) in an FEI Talos F200X equipment supplied by Thermo Fisher Scientific (USA). This equipment combines outstanding high-resolution STEM and TEM imaging. The samples were dispersed in ethanol, and a drop of the suspension was put on a Cu grid (300 mesh).

The textural properties were determined from their N_2 adsorption-desorption isotherms at -196°C, using an ASAP 2020 Micromeritics equipment (USA). In a prior step to the analysis, the samples were outgassed at 200°C and a pressure of 10^{-4} mbar overnight. The specific surface area was determined by the BET method, with a N_2 molecule cross-section of 16.2 Å^2 [22]. The pore size and micropore size distributions were determined by the DFT [23] and MP methods [24], respectively.

The characterization of the clays, before and after the adsorption and after the desorption processes, was evaluated by Fourier Transform Infrared Spectroscopy (FTIR). The samples were prepared in KBr tablets (2 mg of sample + 200 mg of dry KBr) and were analyzed in a Shimadzu FTIR 8300 spectrometer (Japan), in the range 500 to 4000 cm^{-1}.

2.4. Starting Plant. The purple cabbage was obtained from local trade in Fortaleza (Ceará, Brazil), manually cut and freeze-dried in a Labconco Freeze Dry-5 dryer (Labconco, MO) under pressure of 0.6 Pa for 48 h. After drying, the sample was crushed in a domestic blender and sieved on a 700 μm mesh to obtain a powder. The purple cabbage powder was stored (-5°C) in polyethylene bottles until the moment of analysis.

2.5. Anthocyanin Extraction. For ACN extraction, 10 g of purple cabbage was treated with a solution composed of 27 mL of ethanol (80% vol.) and 3 mL of trifluoroacetic acid. The mixture was sonicated (USC-1400; standard ultrasonic frequency of 40 kHz and real power of 135 W) for 20 min, and this process was repeated until the residue was colorless. The extracts obtained were mixed and concentrated at 40°C in a rotavapor R-215 (Bunch, Flawil, Switzerland) under reduced pressure. The crude extract was stored in glass bottles at -5°C until the moment of analysis.

2.6. Anthocyanin Quantification. The quantification of ACNs present in powdered cabbage was performed according to Do et al. [25]. The extracts were solubilized in a potassium chloride buffer (pH 1.0) and sodium acetate (pH 4.5) and read on a BioMate 3 UV-VIS spectrophotometer (Thermo Scientific, USA) in quartz cuvettes (1 mL) at 520 and 700 nm. The buffers were used as blanks. Total anthocyanins (AntT), expressed as a cyanidin-3-glucoside equivalent, were obtained according to the following equation.

$$\mathrm{AntT} = \frac{A \times \mathrm{MM} \times \mathrm{FD} \times 1000}{\varepsilon \times 1}, \quad (1)$$

where A is the absorbance (for differential pH $A = [(A_{520\mathrm{nm}} - A_{700\mathrm{nm}})\mathrm{pH}\,1.0 - (A_{520\mathrm{nm}} - A_{700\mathrm{nm}})\mathrm{pH}\,4.5]$), MM is the molar mass (449.2 g/mol for cyanidin-3-glucoside), FD is the dilution factor, and ε is the extinction coefficient (26900 L/mol/cm). These reading procedures were performed for all samples and at all stages of the experiments.

2.7. Determination of the Point of Zero Charge (pH_{PZC}). The determination of the point of zero charge (pH_{PZC}) of the clays was based on 11 experimental points, as was previously described by Schreider and Regalbuto and Regalbuto and Robles [26, 27]. For these studies, 25 mL of a 0.01 M NaCl solution was distributed in 10 beakers, in which the pH was adjusted in the range of 2 to 11 with hydrochloric acid (HCl) or sodium hydroxide (NaOH). Sequentially, 25 mg of each clay was dispersed in NaCl solutions and kept for 48 h. Finally, the pH of each beaker was measured, and the difference between the initial pH and the final pH was plotted.

2.8. Static Adsorption Experiments. The optimization of the conditions for the ACN adsorption process in natural and modified clays was carried out using batch experiments, at a constant temperature of 22°C. Adsorption studies were performed in a Tecnal rotary agitator (model TE-165, Brazil) at 121 rpm. The ACN extracts and clays were mixed in Falcon tubes (15 mL), and the data were obtained from the contact according to the time defined for each test. At the end of each test, the extracts were separated from the adsorbents using a CT-15000R refrigerated centrifuge (CIENTEC, Brazil) for 10 min at 2540 rpm, and the ACN content was quantified (Equation (1)). Equation (2) was used to calculate the adsorption capacity per gram of adsorbent (mg·g^{-1}):

$$q = \frac{V \times (C_i - C_f)}{m}, \quad (2)$$

where C_i and C_f are the initial and final concentrations in the liquid extract, respectively; q (mg·g^{-1}) is the amount of ACN adsorbed on the solid phase; m (g) is the mass of adsorbent; and V (mL) is the volume of the sample solution.

For the selection of the most suitable clay for the ACN adsorption, 10 mg of each adsorbent was dispersed in 10 mL of the ACN extract, while remaining under agitation for 3 hours at 22°C. After the test, the ACNs were quantified, and the amount adsorbed was calculated according to Equation (2).

Once the clays with the highest adsorption capacity were selected, the mass of adsorbent was optimized. From 10 to 100 mg of each clay was weighed, which was kept in contact with 10 mL of the ACN extract for 3 hours. At the end of the test, the adsorbed ACNs were quantified according to Equation (2).

To determine the amount adsorbed, 25 mg of each clay (mass optimized) was dispersed in 10 mL of extract. Aliquots of supernatant were collected at regular intervals (0, 1, 3, 5, 10, 20, 30 min, and every 30 min until 3 h). The amount of

adsorbed ACNs was determined according to Equation (2), and after each reading, the pH was monitored using a DM-22 pH meter (Digimed, Brazil) to evaluate the influence of pH on the adsorption process. All adsorption experiments were performed at least three times, and no significant deviations (<5%) were observed.

2.9. Static Desorption Experiments. Desorption tests were performed with the following methodology. After ensuring that the adsorption equilibrium was reached, the clays loaded with ACNs were washed with 30 mL of water and then desorbed with 10 mL of ethanol 80% (0.1% *v*/*v* HCl). The tests were performed on a rotary shaker at a constant speed, according to the time determined for each experiment. After each test, the eluted samples were separated from the clays by centrifugation (10 min at 2540 rpm) and analyzed in a spectrophotometer. The percentage of desorption capacity ACNs was calculated using the mass balance presented in the following equation.

$$\%\text{desorption} = \frac{C_{\text{desorption}}}{C_{\text{initial}} - C_{\text{adsorption}}} \times 100, \quad (3)$$

where C_{initial}, $C_{\text{adsorption}}$, and $C_{\text{desorption}}$ are the concentrations of anthocyanins at the beginning, after adsorption, and after desorption, respectively.

2.9.1. Kinetic Study of the Desorption Process. For the kinetic study of the desorption of the ACNs, 10 mL of 80% (*v*/*v*) ethanol was used to perform the desorption of the ACNs. 2 mL aliquots of the solution were removed at regular intervals from 30 to 240 min to assess when the desorption process reached equilibrium. The amount of ACNs desorbed was determined by UV-visible and calculated according to Equation (3).

2.9.2. Evaluation of the Eluent. In order to evaluate the most suitable eluent for the ACN desorption, aqueous solutions of ethanol and methanol (60, 80, and 90%*v*/*v*), acidified with HCl (0.1% *v*/*v*) or not, were tested. The clays were loaded with ACNs, and the solvents were kept under constant agitation for 120 min, as determined in the previous test (Section 2.9.1). The amount of ACNs desorbed was calculated according to Equation (3).

2.10. Quantification of Sugars. Total sugars were quantified in the supernatants after adsorption and desorption tests using the phenol-indole method, as described by Dubois et al. [28]. 0.5 mL of each extract was reacted with 0.5 mL of 5% (*v*/*v*) phenol solution and 2.5 mL of H_2SO_4. After 15 minutes of incubation, the samples were placed in quartz cuvettes and read in a spectrophotometer at 490 nm. Ultrapure water was used as a blank. Quantification was performed using a glucose standard curve, and the results were expressed in mg L^{-1}.

2.11. Analysis of Anthocyanins by HPLC–MS/MS. The ACN extract was characterized by mass spectrometry in a chromatographic system ACQUITY UPLC (Waters, USA), coupled to a Quadrupole Time-of-Flight system (QTof, Waters). The chromatographic runs were performed on a chromatographic column Waters ACQUITY UPLC BEH (150 × 2.1 mm, 1.7 μm) under the following conditions: fixed temperature of 40°C, mobile phase of water with 0.1% formic acid (*A*) and acetonitrile with 0.1% formic acid (*B*), gradient ranging from 2% to 95%*B* (21 min), flow of $0.4\,\text{mL min}^{-1}$, and injection volume of 5 μL. High-resolution mass conditions using a Xevo QTof in positive mode (ESI^+) were acquired in the range of 110-1180 Da, fixed source temperature of 120°C, desolvation temperature of 350°C, flow rate of $500\,\text{L h}^{-1}$, and capillary voltage of 3.2 kV. Leucine enkephalin was used as a *lock mass*. The acquisition mode was MS^{E}. The instrument was controlled by MassLynx software 4.1 (Waters Corporation, USA).

3. Characterization of the Adsorbents

3.1. X-Ray Diffraction (XRD). To evaluate the crystallinity of the clay minerals, X-ray diffractograms of these clays were registered (Figure 1). It should be noted that the crystallinity of clay minerals is relatively low compared to other inorganic compounds since these phyllosilicates are raw materials that have not undergone any purification.

The diffractogram of the Bent sample shows a strong and intense reflection with a maximum located at a 2θ value of 6.80°, which is ascribed to the d_{001} reflection. From this diffraction, it is possible to obtain the basal spacing of the Bent sample through the Bragg equation, obtaining a value of 13.0 Å, so the cation located in the interlayer spacing must be partially hydrated. In the same way, other broad reflections are observed and ascribed to the bentonite. Of these, one of the most interesting diffraction peaks is the d_{060} reflection located at 2θ of 62.05° since it is possible to discern between a trioctahedral and dioctahedral smectite. The presence of the d_{060} reflection at 1.49 nm confirms that the phyllosilicate is dioctahedral, so this adsorbent must be an Al-rich smectite. On the other hand, other narrower reflections are observed, which are ascribed to some impurities (calcite, plagioclase, and cristobalite) [21].

In the case of the Sep sample, its typical diffraction peaks are observed, where the main diffraction peak is located at 2θ of 7.27° (12.1 Å) and is assigned to the d_{110} reflection [29]. In addition, a small quartz impurity located at 2θ of 26.55° is observed. The diffractogram of the Ata sample shows a main peak located at 2θ of 8.37° (10.5 Å), which is ascribed to the typical d_{110} reflection of this clay mineral [30]. Moreover, this sample also displays impurities of quartz.

Finally, the PCH synthesized from bentonite was also studied by XRD. The diffractogram of the PCH reveals that the insertion of Si pillars causes a loss of the nonbasal reflections while the basal reflections (d_{020}, d_{110}, d_{130}, d_{200}, and d_{060}) are maintained although these signals can suffer a random displacement as a consequence of the partial delamination of the clay mineral [31]. On the other hand, the absence of impurities after the formation of the PCH is striking, as was observed in previous studies [19]. The analysis of the low angle of the PCH (Figure 2) reveals the presence of a broad band located about 2θ of 2.60° (33 Å), which confirms

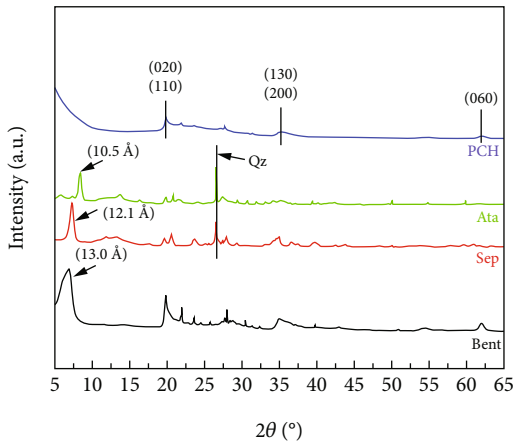

FIGURE 1: X-ray diffractograms of bentonite (Bent), sepiolite (Sep), attapulgite (Ata), and porous clay heterostructure (PCH).

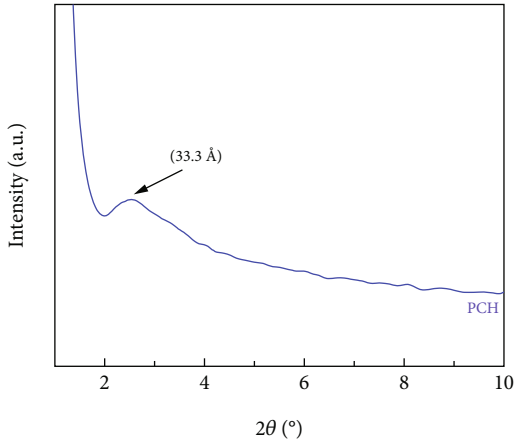

FIGURE 2: Low-angle X-ray diffractogram of the PCH.

the formation of an expanded structure because of the insertion of silica pillars between adjacent sheets to form the PCH structure [21].

3.2. Transmission Electron Microscopy (TEM). The morphology of the raw clays and the PCH was analyzed by TEM (Figure 3). In the case of the Bent sample (Figure 3(A)), the typical lamellar structure of bentonite can be observed. When the pillars are included to form the PCH (Figure 3(B)), the lamellar structure is maintained although a higher disorder of the sheets is observed, confirming that the insertion of pillars causes a partial delamination of the structure [31]. Both the Sep and Ata samples show a fibrous structure (Figures 3(C) and 3(D)). From the TEM, it is not possible to differentiate between both fibrous structures since the difference between them lies in the periodic inversion of the tetrahedral sheet leading to microchannels with the dimensions of 0.37 nm × 1.06 nm for Sep and 0.37 nm × 0.64 nm in the case of Ata [32].

3.3. Textural Properties. The textural properties of the raw clay minerals and the PCH were determined from N_2 adsorption-desorption isotherms at -196°C (Figure 4). According to the IUPAC classification, the isotherms of both raw clay minerals and PCH can be adjusted to type II, which are typical of materials with high macroporosity due to the voids between adjacent particles [33]. Regarding the hysteresis loops, the isotherm can be fitted to type H3, which is typical of nonrigid aggregates of plate-like particles as clay minerals [33]. In the case of the raw clays, it can be observed how the N_2-adsorbed at low relative pressure is relatively low, which suggests that these materials display low microporosity. These data are striking for the fibrous phyllosilicates (Sep and Ata) since these clays display nanocavities, which are very efficient for retaining small molecules such as CO_2 [32]. In these fibrous phyllosilicates, N_2-adsorption values increase remarkably at a high relative pressure. This supposes that both materials display high macroporosity probably due to voids between adjacent fibers. The analysis of the adsorption isotherm of the Bent sample shows how the N_2 adsorption is lower than that observed for both fibrous phyllosilicates, so it is expected that the Bent sample shows poorer textural properties than the other raw clays. However, the substitution of the cation located in the interlayer spacing by a bulkier organic cation and the formation of pillared structures such as PCH lead to structures with higher porosity. Thus, the PCH sample shows a clear increase in N_2 adsorption at low relative pressures, so an increase in microporosity is expected, probably due to the partial delamination of the clay mineral in the pillaring step and its subsequent calcination leading to a microporous structure due to the formation of a house-of-cards structure [31]. This delamination also gives rise to the formation of macroporosity, as suggested by the increase in N_2 adsorption at a high relative pressure.

The estimation of the mesoporosity was carried out by the BET equation (Table 1) [22]. BET surface area (S_{BET}) values reveal how the raw clay with the highest surface area and higher microporosity is Sep due to the presence of zeolitic channels. In the case of the other fibrous clays (Ata), it can be observed how this sample displays lower meso- and microporosities. In this sense, it has been reported in the literature that Sep can host a higher proportion of small molecules, such as CO_2, in its zeolitic channels than Ata [32]. The synthesis of the PCH improves textural properties compared to its respective starting bentonite. Thus, it can be observed how PCH displays a BET surface area of 640 $m^2 g^{-1}$ and a pore volume of 0.828 $cm^3 g^{-1}$. In addition, the *t*-plot data also reveals that PCH displays high microporosity than the raw bentonite [21]. These data confirm that the incorporation of PCH promotes the formation of micro-, meso-, and macropores.

The estimation of the pore size distribution was carried out by the DFT method (Figure 5) [23]. This figure shows how all raw clays display a wide pore distribution due to the variable porosity ascribed to the voids between adjacent particles. However, in the case of the PCH, the presence of a narrow distribution with two maxima can be observed. The first maximum located at 1.9 nm is probably attributed to the microporosity generated in the synthesis of the PCH, and a second maximum, located about 3.0 nm, is

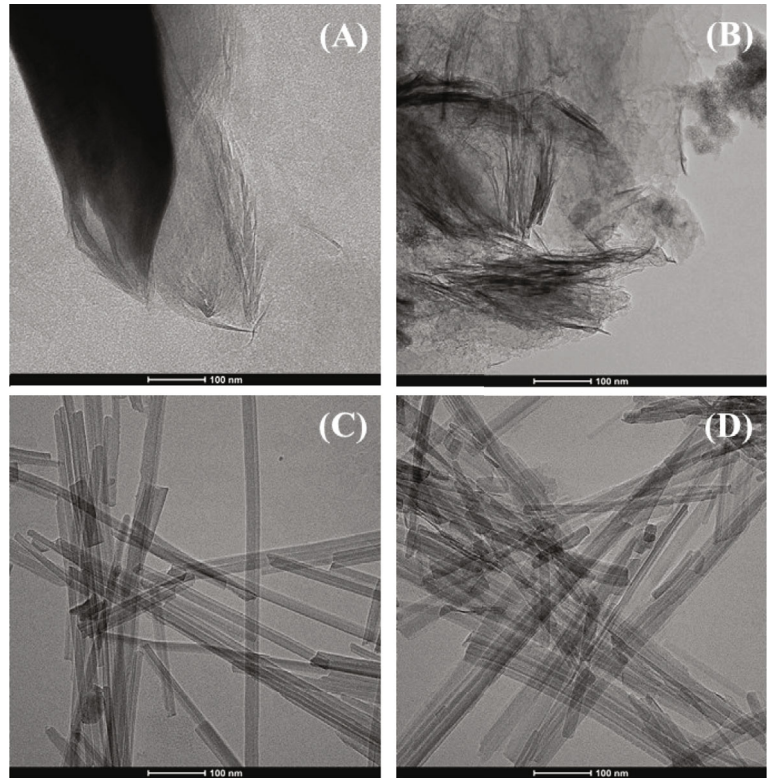

Figure 3: TEM micrographs of Bent (A), PCH (B), Sep (C), and Ata (D).

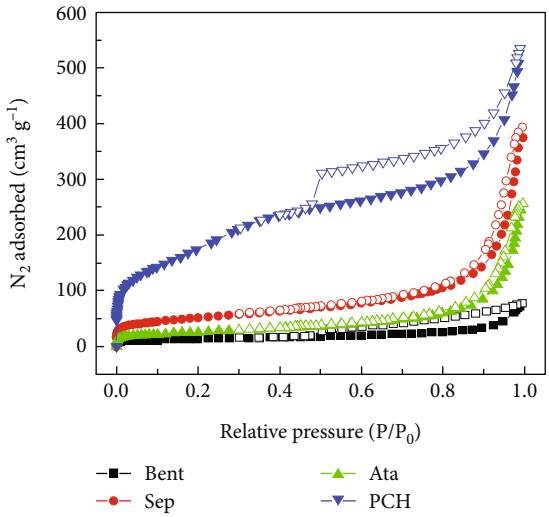

Figure 4: N_2 adsorption-desorption isotherms at -196°C of Bent, Sep, Ata, and PCH.

ascribed to the porosity generated in the pillared process and the delamination of the clay. This value seems to agree with that data obtained for low-angle XRD (Figure 2).

3.4. Attenuated Total Reflectance (ATR). Both the raw clay and the PCH obtained from the Bent sample were also characterized by ATR (Figure 6(a)). The study of the -OH stretching region, compiled in Figure 6(a), shows how the Bent sample displays a broad band located about 3630 cm^{-1}, which is assigned to the Al(OH)Al stretching vibration mode, which is typical of Al-rich smectites [34, 35]. In addition, the presence of a small contribution close to 3700 cm^{-1} also draws attention, which suggests the existence of pyrophyllite-like local structural fragments [34]. In the case of the Sep sample, two bands located at 3690 and 3625 cm^{-1} are observed [32, 36], which are assigned to -OH stretching vibration modes coordinated with Mg^{2+} species, while the band located at 3670 cm^{-1} is assigned to the H_2O stretching vibration mode coordinated with Mg^{2+} species [36].

Regarding the Ata sample, Frost et al. pointed out that this clay mineral exhibits two bands located at 3616 and 3552 cm^{-1}, which are assigned to the -OH stretching vibration modes of Mg^{2+} and Al^{3+} or Fe^{3+} species, respectively [36]. In both fibrous clays (Sep and Ata), two other bands located about 3400 and 3250 cm^{-1} are attributed to the physisorbed H_2O in the nanocavities [32]. The study of the PCH sample shows how the band located about 3630 cm^{-1} disappears due to the thermal treatment in the calcination step, causing a partial dehydroxilation of the Al-rich smectite [21]. The absence of a band about 3740 cm^{-1} is also

Table 1: Textural properties of Bent, Sep, Ata, and PCH samples estimated from N_2 adsorption-desorption isotherms at -196°C.

Sample	S_{BET} ($m^2\,g^{-1}$)	t-plot$_{mic}$ ($m^2\,g^{-1}$)	t-plot$_{ext}$ ($m^2\,g^{-1}$)	V_P ($cm^3\,g^{-1}$)
Bent	48	14	21	0.119
Sep	182	48	134	0.608
Ata	93	13	80	0.397
PCH	640	376	264	0.828

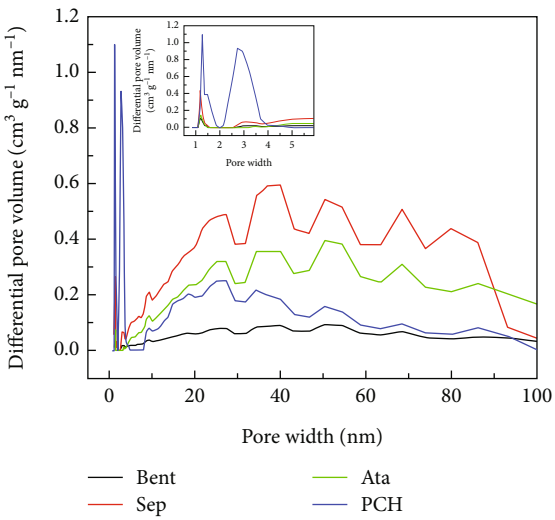

FIGURE 5: Pore size distribution of Bent, Sep, Ata, and PCH.

noticeable, discarding the presence of silanol groups in the SiO_2 pillars because the pyrolytic treatment promotes the dehydroxylation of the silanol groups into siloxane.

The analysis of the region between 2000 and 500 cm^{-1} (Figure 6(b)) for the Bent sample shows a broad band with a maximum located at 1030 cm^{-1}, which is assigned to the Si-O stretching mode [37]. The band located at 918 cm^{-1} is attributed to the Al_2OH bending mode, while the shoulder located about 884 cm^{-1} is attributed to the AlMgOH bending mode due to the partial substitution of Al by Mg species. The small contributions located about 793 and 693 cm^{-1} are assigned to Fe_2OH and Fe–O out-of-plane vibration modes, indicating that Fe^{3+} must be partially replacing Al^{3+} species. Finally, the bands located at 525 and 465 cm^{-1} are assigned to Si-O-Al and Si–O–Si bending vibrations, respectively [37].

In the case of the Sep sample, the set of bands between 1230 and 850 cm^{-1} is assigned to the Si-O stretching mode. In the same way, the bands located about 785 cm^{-1} and 470 cm^{-1} are assigned to the Si-O-Si symmetric stretching vibration and Si-O-Si bending mode, respectively. The band located at 660 cm^{-1} is assigned to the Mg_3OH bending vibration mode, while the band about 425 cm^{-1} is attributed to the Si-O-Mg bending vibration mode. For the Ata sample, a band located at 515 cm^{-1} can also be observed, to which the Si-O-Al bending vibration mode is assigned [32, 38].

For the PCH sample, the incorporation of the SiO_2 pillar causes a shift of the band ascribed to the Si-O stretching mode to higher wavenumber values. In the same way, the broad bands close to 975 cm^{-1} (Si-O in-plane stretching vibration mode) and 805 and 470 cm^{-1} (bending vibration modes) also confirm the presence of SiO_2 in the form of pillars [39], as suggested from XRD (Figure 2) and textural property data (Figures 4 and 5).

Finally, a broad band at 1630 cm^{-1} is observed for all samples. This band is assigned to the H–O–H bending mode band, which is typical of the physisorbed H_2O.

4. Adsorption Studies

From the dilution of the concentrated crude extract, a solution of ACNs with a concentration equal to 40 $mg{\cdot}L^{-1}$ was prepared using ultrapure water as the diluent. This solution presented a concentration of sugars equal to 2283.7 $mg{\cdot}L^{-1}$. The prepared volume was sufficient to carry out all experiments.

4.1. Selection of Adsorbents. It is well-known that phyllosilicates are materials with high cation exchange capacity and high adsorption capacity for organic molecules. Thus, these adsorbents can be potential hosts to ACNs. As shown in Figure 7, the PCH sample displays a high adsorption capacity for ACNs ($q = 16.89\ mg\ g^{-1}$), adsorbing approximately 42% of the pigments in the solution. This result did not differ statistically ($P > 0.05$) from that presented by the Sep sample (16.64 $mg\ g^{-1}$), which has reached an adsorption capacity of 41%. The lowest values were observed for the Ata sample, which only adsorbs 27.4% of the pigments.

The results obtained for the PCH and Sep samples are directly related to their structural properties (Table 1). For the PCH sample, the formation of a pillared and delaminated adsorbent with high micro- and mesoporosity results in a greater ACN adsorption [40, 41]. In the case of the Sep sample, the fibrous morphology with a crystalline structure, with high specific surface area and high porosity (Table 1), results in a high capacity for adsorption of dyes, organic compounds, and other substances [42, 43]. On the other hand, the smaller surface area obtained by the Bent and Ata samples seems to be related to the lowest observed ACN adsorption values. Thus, considering the amount of ACNs adsorbed, the PCH and Sep samples were selected to perform the other adsorption tests.

4.2. Influence of the Mass in the Adsorbent Test. The data reported in Figure 8 show how the amount of adsorbed ACNs increased proportionally with the increasing mass of the adsorbent; however, this increase was nonlinear for the PCH sample. The ratio between the mass of adsorbed ACNs and the mass of adsorbent showed that, in terms of process economy, 25 mg of clay was sufficient for the effective adsorption of ACNs, which was equal to 0.096 and 0.180 mg for Sep and PCH samples, respectively. From these results, it was possible to evaluate the most suitable mass of clay for the adsorption of ACNs from the cabbage extract, which is, in general, an important result to determine the maximum adsorption capacity and the economy of the process.

4.3. Equilibrium Conditions for the Adsorbents. It can be observed that adsorption of ACNs in Sep and PCH occurred quickly after the first few minutes of the process (Supplementary Information, Figure S1). For the Sep sample, equilibrium conditions were reached after the third minute, obtaining a relationship between the initial concentration (C_0) and the final concentration (C_f) of $C_0/C_f = 0.77$. Using a longer adsorption time causes a slight increase in adsorption, showing an initial to final

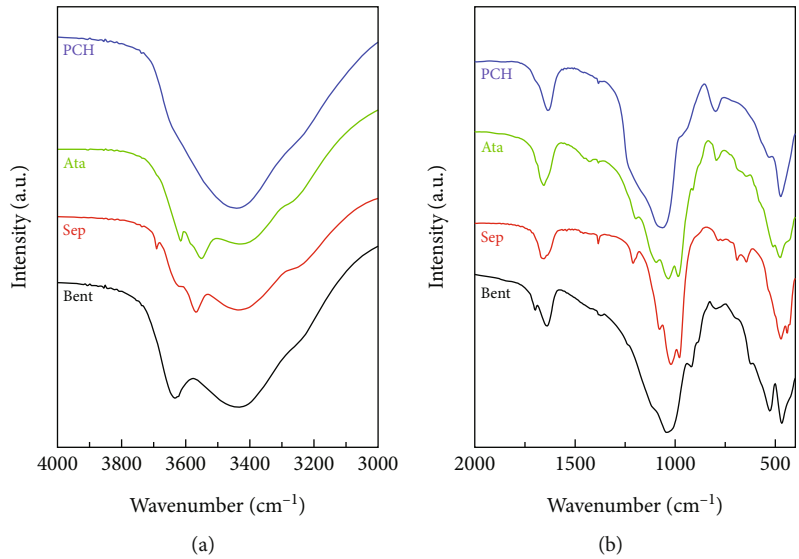

Figure 6: ATR of Bent, Sep, Ata, and PCH in the region 4000-3000 cm^{-1} (a) and 2000-400 cm^{-1} (b).

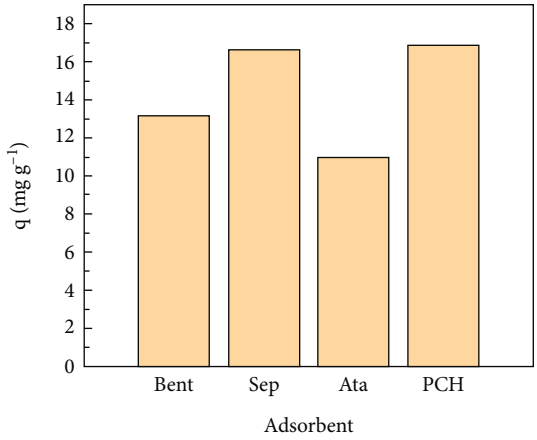

Figure 7: Amount of ACNs adsorbed (q) in different natural and modified clays after 3 hours of contact during the adsorbent selection test.

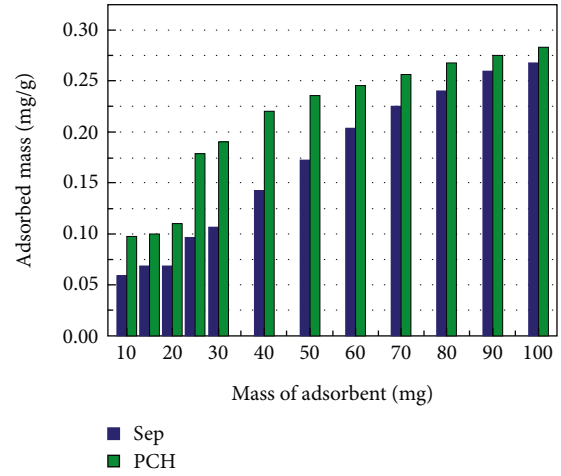

Figure 8: Mass of ACNs adsorbed in different amounts of Sep and PCH.

concentration ratio of 0.66 after 300 minutes. For PCH, it is noteworthy that the adsorption is more progressive. Thus, the adsorption curve presents an intense decrease, going from 0.46 after 3 min to 0.298 at 120 min, when the equilibrium was reached. The PCH showed great potential for adsorption, around 70.2% of ACNs after 120 minutes of processing. However, Sep only adsorbs 35% of the ACNs after 300 min. The obtained results from the PCH samples are above those obtained by Lopez et al. [8], who achieved an adsorption of about 35% of the ACNs, using a similar initial concentration of purple cabbage (*Brassica oleracea* var. Capitata) and using commercial clays as adsorbent.

The ACN adsorption mechanism process on clays can be explained by the behavior of the system in the solution. Previous studies have reported that the exposition of the clay minerals to a polar solvent, such as H_2O, promotes negative electrical charges on the surface of the sheets through different mechanisms (e.g., dissociation of groups or dissolution of surface ions and uniform adsorption) [44]. As ACNs take the form of flavylium cations in moderately acidic conditions, some authors have reported that fast adsorption should take place with the negative charges of the sheets [45]. On the other hand, the higher adsorption capacity of PCH compared to the Sep sample must also be attributed to its textural properties. The presence of high microporosity allows hosting a higher proportion of ACNs in narrow pores due to electrostatic interactions.

4.4. Influence of the pH in the Adsorption Process. The pH is a critical factor in the adsorption process between the ACNs and the clays, so this parameter was monitored during the assays. Abrupt pH changes have not been detected in the samples containing Sep and PCH. However, a different behavior was observed for each one. For the Sep sample, the pH value increases slightly from the beginning (pH = 3.91) to the end (pH = 4.70) when equilibrium is reached (300 min). This increase suggests that Sep has the

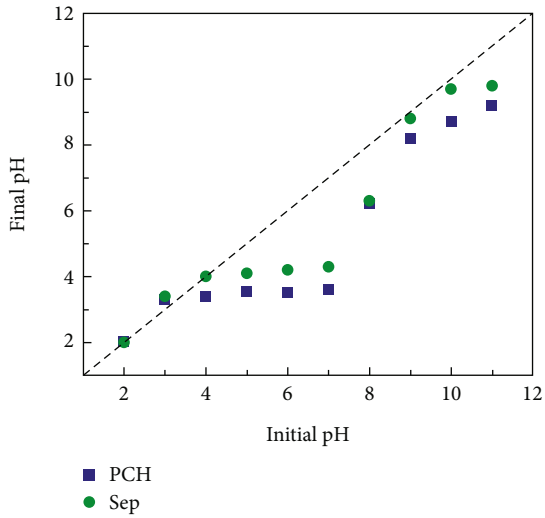

Figure 9: pH of zero charge (pH_{PZC}) of the Sep and PCH samples.

potential to retain H^+ species, so it can be plausible that adsorption on sepiolite could take place between the flavylium cations and the fibers, which are negatively charged on their surface [45].

In the case of the PCH sample, the variation presents a slight decrease, reaching a pH of 3.23 after the equilibrium time (300 min). This suggests that the adsorption process must follow a different mechanism than that in the case of the Sep sample. In this sense, it has previously been reported that the decay in pH could be ascribed to the compensation of unbalanced charges in the ACN and clay structures [8, 46]. As the pH after the adsorption process has not increased, the presence of another type of interaction, alternative to the ionic, is also possible. In this sense, the interaction between the PCH and ACNs through other electrostatic interactions in narrow micropores is also possible.

4.5. Study of the Point of Zero Charge (pH_{PZC}). To determine the pH of the zero charge (pH_{PZC}) point of the clays, the pH_{PZC} value was calculated from the difference between the initial and final pH. Figure 9 reveals that the PCH presented its pH_{PZC} at 3.4, while the Sep sample reaches pH_{PZC} at 4.0. This value indicates the pH value at which there is a balance between the positive and negative charges on the surface of these adsorbents. Thus, for pH values lower than pH_{PZC}, PCH and Sep present a positive surface charge, leading to a higher affinity for anionic groups. When the pH is higher than pH_{PZC}, the surface of these clays has a negative surface charge and therefore a higher affinity for cationic groups. Considering that the pH of the plant extract used in the adsorption is around 3.9, the ACNs are in the form of flavylium cation. At this pH value, ACNs are positively charged, while the Sep sample must be negatively charged although this value is very close to the pI, so the Sep sample should be barely charged at that pH value. Under these conditions, the presence of ionic interactions between the ACNs positively charged and the surface of the clay layers together with other interactions as hydrogen bonds should be expected [47]. In the case of the PCH sample, the adsorbent

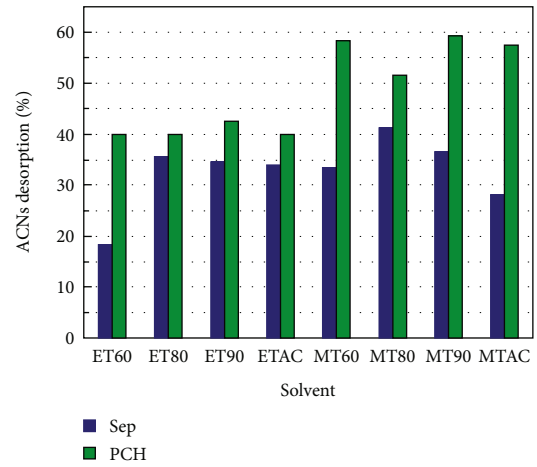

Figure 10: Percentage of ACNs desorbed in relation to the concentration adsorbed by the PCH and Sep, modifying the proportion of eluents (ethanol and methanol) and their concentrations (ET60: ethanol 60%; ET80: ethanol 80%; ET90: ethanol 90%; ETAC: acidified ethanol; MT60: methanol 60%; MT80: methanol 80%; MT90: methanol 90%; MTAC: acidified methanol).

is positively charged while the ACNs are also positively charged. This should cause repulsive interactions so the adsorption must follow another type of interaction. In this sense, the high surface area and high micro- and mesoporosity of the PCH sample should capture ACN molecules in its porous structure [48].

4.6. Desorption Studies. For the desorption process, the best conditions obtained in the adsorption stage were reproduced. Thus, the desorption data have been obtained based on the percentages of adsorbed ACNs (i.e., 70% or 28.0 $mg{\cdot}L^{-1}$ in PCH and 35% or 14 $mg{\cdot}L^{-1}$ in Sep).

In the first stage, it was observed that the ACN desorption was proportional to time for both clays. Even with similarity, the desorption of ACNs in the PCH adsorbent shows better results in the range of time evaluated. The greatest desorption occurred at 120 minutes, where 40% of the ACNs was desorbed (11 $mg{\cdot}L^{-1}$). Under the same conditions, 36% of the ACNs (5.04 $mg{\cdot}L^{-1}$) of the Sep sample was desorbed.

Figure 10 shows the desorption profiles of the ACNs using different amounts of ethanol and methanol. For the Sep sample, the best results have been attained using ethanol (4.97 $mg\,L^{-1}$) and methanol (5.77 $mg\,L^{-1}$), at a concentration of 80% (*v*/*v*). The Sep sample eluted with ethanol 60% presented the lowest desorption percentage (18%), while the others presented values above 28%. For the PCH, the best results were obtained using methanol as the eluent, in concentrations of 60 and 90%, which reached about 60% of desorption (16.40 and 16.60 $mg\,L^{-1}$, respectively). In the case of ethanol, the PCH samples showed a similar desorption pattern, varying between 39.90% (11.17 $mg\,L^{-1}$) and 42.60% (11.92 $mg\,L^{-1}$). Considering that all the samples eluted with methanol presented a desorption capacity higher than those eluted with ethanol, PCH (60% methanol) was chosen as the eluent, as it presented a capacity of desorption equal to

58.60% (16.40 mg L^{-1}). In addition, it was also observed that the acidification of the eluent did not influence the desorption in both cases.

On the other hand, it is also noticeable that desorption is less efficient in the case of Sep. These data suggest that the interaction between ACNs and Sep, which must be partially ionic, is stronger than that observed between ACNs and PCH, despite that ACN molecules must be captured in the porous structure.

4.7. Quantification of Sugars. Compared to the concentration of the initial solution, the solutions that remained after the adsorption process present a high concentration of sugars (89.56% for the Sep sample and 81.05% for the PCH sample), showing that the clays did not adsorb a large amount of this set of molecules. This result suggests that the affinity of the ACNs for the adsorbent is higher and faster than that of sugars. In this sense, sugars are also bulkier than ACNs, which is also difficult for their adsorption. In both clays, the solutions obtained after desorption showed a sugar concentration of only 2% of the initial content, indicating that the clays showed good selectivity related to ACNs. In this sense, previous authors reported a concentration of sugar less than 0.1% compared to their initial extract using macroporous resins for the purification of the ACNs extracted from purple cabbage (*Brassica oleracea* var. Capitata) and jambolan fruit (*Syzygium cumini* L.) [49, 50].

4.8. Anthocyanin Identification. The UPLC-QToF analyses, carried out in the positive ionization mode, allowed identification of the compounds present in the purple cabbage extract before and after the adsorption process on the clays, as well as in the desorption. Peaks identified in the PCH (Supplementary Information, Figure S2A) and Sep (Supplementary Information, Figure S2B) chromatograms were labeled according to the order of elution. In Table 2, it is possible to find six identified compounds, their protonated ions and their ionic fragments, as well as the error in parts per million (ppm) and their possible molecular formula. The extracted ACNs are listed below.

Peak 1 (rt = 2.244 min) represents cyanidin-3-diglucoside-5-glucoside, and its structure is the basis for the composition of the other ACNs, as was previously reported by other authors [51]. Beside the position and quantity of sugars, the bonds with phenolic acids, such as synaptic (peaks 2 and 5), ferulic (peaks 3, 4, and 5), and coumaric (peak 2) acids, characterized the structural difference of ACNs. The identification of these acids in the structure was facilitated due to the presence of their characteristic fragments [52, 53].

All the ACNs identified in this study are acylated and derived from cyanidin-3-diglucoside-5-glucoside (m/z 773), which is in agreement with other studies carried out for other cabbage species [54–56]. This is confirmed by tandem mass spectrometry (MS/MS) of the molecular ions having the fragments m/z 449 or m/z 611, which represent the residues of cyanidin-5-glucoside and cyanidin-3-diglucoside, respectively [56], as well as the fragment m/z 287, which corresponds to cyanidin [56].

Peak 2 (rt = 3.889 min), with m/z 919, shows the fragments of ions m/z 757, due to the loss of a hexose, and m/z 449 and m/z 287, which are characteristic of cyanidin [57]. The presence of these fragments indicates the possibility of coumaric acid in the structure of the pigment; thus, the compound was identified as cyanidin-3-(p-coumaroyl)-diglucoside-5-glucoside [2].

Peak 3 (rt = 4.006 min) indicates the presence of two compounds, which possibly coeluted. The first compound showed m/z 979 with the presence of fragments, m/z 449 and m/z 287, and also m/z 817, referring to the loss of a glucose molecule [58, 59]. The ANCs were identified as cyanidin-3-(sinapoyl)-diglucoside-5-glucoside [54]. The second compound (mass spectrum m/z 949) presents a fragment with m/z 287, common to cyanidins, being identified as cyanidin-3-(feruloyl)-diglucoside-5-glucoside. For peak 4 (rt = 4.292 min), the ion fragmentation in m/z 1125 produced ions m/z 963 related to the loss of a glucosyl residue, m/z 449 for the loss of diglucosyl, and m/z 287 of the cyanidins. These fragments indicated the presence of two ferulic acids in the ACN structure, corresponding to the compound cyanidin-3-(feruloyl)(feruloyl)-diglucoside-5-glucoside [2, 60].

Peak 5 (rt = 4.354 min) presents a mass spectrum m/z 1155. The presence of fragments m/z 993, m/z 449, and m/z 287 is observed. This compound was identified as cyanidin-3-(sinapoyl)(feruloyl)-diglucoside-5-glucoside, due to the presence of synaptic and ferulic acids [59, 60].

When comparing the chromatograms of the initial, postadsorption, and postdesorption phases (Supplementary Information, Figure S2A), striking differences are observed between the intensities of the peaks in the samples. Analyzing in terms of concentration and intensity from the overlapping of the peaks, the compound cyanidin-3-diglucoside-5-glucoside (rt = 2.254 min) is more evident in the postadsorption step. However, this compound is less evident in the postdesorption phase, indicating that a low concentration of these ACNs was adsorbed and, consequently, recovered from the PCH.

The behavior of peak 2 (rt = 3.889 min) indicates that a considerable amount of cyanidin-3-(p-coumaroyl)-diglucoside-5-glucoside was adsorbed and recovered from the PCH. This result is evidenced by the intense decrease in the intensity of this peak from the first to the second stage, intensifying again in the last stage.

The compounds coeluted in peak 3 (rt = 4.006 min), cyanidin-3-(sinapoyl)-diglucoside-5-glucoside and cyanidin-3-(feruloyl)-diglucoside-5-glucoside, did not have large amounts adsorbed, once the peak in the second stage showed a slight decrease. However, a reduced amount of these adsorbed ACNs was recovered since the peak is also evidenced in the postdesorption stage.

Most of the ACNs adsorbed and recovered, possibly, were cyanidin-3-(feruloyl)(feruloyl)-diglucoside-5-glucoside (peak 4, rt = 4.292 min) and cyanidin-3-(sinapoyl)(feruloyl)-diglucoside-5-glucoside (peak 5, rt = 4.354 min). Both compounds were more evident in the recovery profiles (postdesorption stage), while in the postadsorption stage, they were less apparent. Unlike the other compounds identified in the chromatogram, these ACNs present two organic

Table 2: Constituents identified or tentatively identified in the ACN extract of red cabbage.

Peak	rt (min)	[M+] (m/z)		Ion fragments (m/z)	Error (ppm)	Molecular formula	Compound	Ref.
		Observed	Calculated					
1	2.254	773.2140	773.2150	611/449/287	1.3	$C_{33}H_{41}O_{21}$	Cyanidin-3-diglucoside-5-glucoside	[54]
2	3.889	919.2508	919.2525	757/449/287	1.5	$C_{42}H_{47}O_{23}$	Cyanidin-3-(p-coumaroyl)-diglucoside-5-glucoside	[54]
3	4.006	979.2719	979.2745	817/449/287	2.1	$C_{44}H_{51}O_{25}$	Cyanidin-3-(sinapoyl)-diglucoside-5-glucoside	[54]
3	4.006	949.2628	949.2630	287	1.5	$C_{43}H_{49}O_{24}$	Cyanidin-3-(feruloyl)-diglucoside-5-glucoside	[51]
4	4.292	1125.3087	1125.3149	963/449/287	5.5	$C_{53}H_{57}O_{27}$	Cyanidin-3-(feruloyl)(feruloyl)-diglucoside-5-glucoside	[53]
5	4.354	1155.3193	1155.3282	993/287/449	7.9	$C_{54}H_{59}O_{28}$	Cyanidin-3-(sinapoyl)(feruloyl)-diglucoside-5-glucoside	[51]

acids in their structure (ferulic or synaptic). Thus, these ACNs have a higher number of hydroxyl and carboxylic groups in their structure, which may promote a better interaction between the ACNs and the sheets and the SiO_2 pillars of the adsorbent surface through electrostatic interactions [61].

For the Sep sample (Supplementary Information, Figure S2B), the adsorption and desorption profiles indicated that this clay does not present a good affinity for the compounds referring to peaks 1, 2, and 3, since their intensity hardly shows considerable changes between the beginning and postadsorption stages. However, there is a lower intensity of these peaks in the postdesorption stage, indicating that these ACNs were recovered from the Sep sample. Regarding peaks 4 and 5, their intensities decreased from the first to the second stage and are quite apparent in the last stage, showing that a large part of these compounds is desorbed on the Sep sample, and therefore, these ACNs are recovered.

5. Conclusions

Several clay minerals have been selected for the recovery and elution of ACNs from purple cabbage to a subsequent valorization. The results obtained in this research showed that the best conditions to adsorb ACNs were obtained using PCH as the adsorbent, and the higher adsorption properties of this clay were related to its higher surface area and pore volume. The 60% methanol solution was found as the best eluent, allowing the recovery a large amount of ACNs adsorbed on PCH. Both the PCH and the sepiolite exhibited a high selectivity for ACNs and a low affinity for the sugars present in the ACN crude extract, facilitating the recovery of these pigments free of possible contaminants. The analysis of the samples by UPLC-QToF and FTIR indicated that the profile of anthocyanins present in purple cabbage is composed of different cyanidin species and that those with more than one organic acid in their structure had a higher affinity for clay, as well as a higher recovery rate. This research was aimed at evaluating the best operating conditions in a simple batch process to obtain a partially purified anthocyanin extract and obtain important results, which will serve as the basis for future research based on the application of anthocyanins and their purified form.

Data Availability

The authors confirm that all data generated or analyzed during this study are available from the corresponding author. These materials can be requested directly from the corresponding author if needed.

Conflicts of Interest

The authors declare that they have no conflicts of interest.

Acknowledgments

This publication is part of the R&D project PID2021-126235OB-C32 funded by MCIN/AEI/10.13039/501100011033/ and FEDER funds and R&D project TED2021-130756B-C31 funded by MCIN/AEI/10.13039/501100011033/ and European Union Next Generation funds. The authors also thank Conselho Nacional de Desenvolvimento Científico e Tecnológico (CNPq, Ministério da Ciência, Tecnologia, Inovações e Comunicações, Brazil) for its financing support.

Supplementary Materials

The supplementary information contains the kinetic studies of Sep and PCH (Figure S1) and the chromatograms of anthocyanins in the purple cabbage extract and their respective chromatograms postadsorption and postdesorption in PCH (Figure S2A) and in sepiolite (Figure S2B). *(Supplementary Materials)*

References

[1] S. Oancea and Z. M. Linn, "Anthocyanins: powerful natural antioxidant pigments with significant biomedical and technological applications," *Oxidation Communications*, vol. 41, no. 1, pp. 92–106, 2018.

[2] J. Zhang, Z. Wang, and X. Liu, "Characterization of acylated anthocyanins in red cabbage via comprehensive two-dimensional high performance liquid chromatography and HPLC-MS," *Journal of Food Processing and Preservation*, vol. 41, no. 2, Article ID e13129, 2017.

[3] L. M. Soldatkina and V. O. Novotna, "Adsorption removal of anthocyanins from red cabbage extracts by bentonite: statistical analysis of main and interaction effects," *Chemistry, Physics and Technology of Surface*, vol. 8, no. 4, pp. 439–447, 2017.

[4] P. Ongkowijoyo, D. A. Luna-Vital, and E. González de Mejía, "Extraction techniques and analysis of anthocyanins from food sources by mass spectrometry: an update," *Food Chemistry*, vol. 250, pp. 113–126, 2018.

[5] T. J. Lopez, S. R. Yaginuma, M. G. N. Quadri, and M. B. Quadri, "Evaluation of red cabbage anthocyanins after partial purification on clay," *Brazilian Archives of Biology and Technology*, vol. 54, no. 6, pp. 1349–1356, 2011.

[6] A. Kraemer-Schafhalter, H. Fuchs, and W. Pfannhauser, "Solid-phase extraction (SPE)—a comparison of 16 materials for the purification of anthocyanins from *Aronia melanocarpa* var Nero," *Journal of the Science of Food and Agriculture*, vol. 78, no. 3, pp. 435–440, 1998.

[7] X. Liu, G. Xiao, W. Chen, Y. Xu, and J. Wu, "Quantification and Purification of Mulberry Anthocyanins with Macroporous Resins," *BioMed Research International*, vol. 2004, Article ID 713759, 6 pages, 2004.

[8] T. J. Lopez, M. G. N. Quadri, and M. B. Quadri, "Recovery of anthocyanins from red cabbage using sandy porous medium enriched with clay," *Applied Clay Science*, vol. 37, no. 1-2, pp. 97–106, 2007.

[9] M. F. Ávila, L. C. Lima, and T. J. Lopes, "Adsorption of red cabbage dye through Pequi coat charcoal (*Cariocar brasiliense*)," *Revista Electronica en Gestado, Educaçao e Tecnología Ambiental*, vol. 19, no. 2, pp. 1561–1573, 2015.

[10] D. Cheikh, H. Majdoub, and M. Darder, "An overview of clay-polymer nanocomposites containing bioactive compounds for food packaging applications," *Applied Clay Science*, vol. 216, article 106335, 2022.

[11] J. A. Cecilia, C. García-Sancho, E. Vilarrasa-García, J. Jiménez-Jiménez, and E. Rodríguez-Castellón, "Synthesis, characterization uses and applications of porous clays heterostructures: a review," *Chemical Record*, vol. 18, no. 7-8, pp. 1085–1104, 2018.

[12] M. Suárez and E. García-Romero, "Advances in the crystal chemistry of sepiolite and palygorskite," *Developments in Clay Science*, vol. 3, pp. 33–65, 2011.

[13] M. Suárez, J. García-Rivas, E. García-Romero, and N. Jara, "Mineralogical characterisation and surface properties of sepiolite from Polatli (Turkey)," *Applied Clay Science*, vol. 131, pp. 124–130, 2016.

[14] Z. Xu, H. Jiang, Y. Yu et al., "Activation and β-FeOOH modification of sepiolite in one-step hydrothermal reaction and its simulated solar light catalytic reduction of Cr(VI)," *Applied Clay Science*, vol. 135, pp. 547–553, 2017.

[15] A. Gil, S. A. Korili, and M. A. Vicente, "Recent advances in the control and characterization of the porous structure of pillared clay catalysts," *Catalysis Reviews*, vol. 50, no. 2, pp. 153–221, 2008.

[16] A. Galarneau, A. Barodawalla, and T. J. Pinnavaia, "Porous clay heterostructures formed by gallery-templated synthesis," *Nature*, vol. 374, no. 6522, pp. 529–531, 1995.

[17] J. E. Aguiar, J. A. Cecilia, P. A. S. Tavares et al., "Adsorption study of reactive dyes onto porous clay heterostructures," *Applied Clay Science*, vol. 135, pp. 35–44, 2017.

[18] M. D. Soriano, J. A. Cecilia, A. Natoli, J. Jiménez-Jiménez, J. M. López-Nieto, and E. Rodríguez-Castellón, "Vanadium oxide supported on porous clay heterostructure for the partial oxidation of hydrogen sulphide to sulfur," *Catalysis Today*, vol. 254, no. 1, pp. 36–42, 2015.

[19] E. Vilarrasa-García, J. A. Cecilia, D. C. S. Azevedo, C. L. Cavalcante Jr., and E. Rodríguez-Castellón, "Evaluation of porous clay heterostructures modified with amine species as adsorbent for the CO_2 capture," *Microporous Mesoporous Materials*, vol. 249, no. 1, pp. 25–33, 2017.

[20] M. V. Villar, L. Pérez del Villar, P. L. Martín et al., "The study of Spanish clays for their use as sealing materials in nuclear waste repositories: 20 years of progress," *Journal of Iberian Geology*, vol. 32, no. 1, pp. 15–36, 2006.

[21] J. A. Cecilia, C. García-Sancho, and F. Franco, "Montmorillonite based porous clay heterostructures: influence of Zr in the structure and acidic properties," *Microporous and Mesoporous Materials*, vol. 176, pp. 95–102, 2013.

[22] S. Brunauer, P. H. Emmett, and E. Teller, "Adsorption of gases in multimolecular layers," *Journal of American Chemical Society*, vol. 60, no. 2, pp. 309–319, 1938.

[23] J. Landers, G. Y. Gor, and A. V. Neimark, "Density functional theory methods for characterization of porous materials," *Colloids and Surfaces A: Physicochemical and Engineering Aspects*, vol. 437, pp. 3–32, 2013.

[24] R. S. Mikhail, S. Brunauer, and E. E. Bodor, "Investigations of a complete pore structure analysis," *Journal of Colloid and Interface Science*, vol. 26, no. 1, pp. 45–53, 1968.

[25] J. R. Do, H. K. Kim, H. K. Kim, J. H. Hong, and G. D. Lee, "Optimization of extraction conditions for cabbage," *Journal of the Korean Society of Food Science and Nutrition*, vol. 34, no. 10, pp. 1625–1632, 2005.

[26] M. Schreider and J. R. Regalbuto, "A fundamental study of Pt tetraammine impregnation of silica. 1. The electrostatic nature of platinum adsorption," *Journal of Catalysis*, vol. 225, no. 1, pp. 190–202, 2004.

[27] J. R. Regalbuto and J. Robles, *The Engineering of Pt/Carbon Catalyst Preparation*, University of Illionis, Chicago, IL, USA, 2004.

[28] M. Dubois, K. A. Gilles, J. K. Hamilton, P. A. Rebers, and F. Smith, "Colorimetric method for determination of sugars and related substances," *Analytical Chemistry*, vol. 28, no. 3, pp. 350–356, 1956.

[29] F. Franco, M. Pozo, J. A. Cecilia, M. Benítez-Guerrero, E. Pozo, and J. A. Martín-Rubí, "Microwave assisted acid treatment of sepiolite: the role of composition and "crystallinity"," *Applied Clay Science*, vol. 102, pp. 15–27, 2014.

[30] L. Pardo-Canales, S. Essih, J. A. Cecilia et al., "Modification of the textural properties of palygorskite through microwave assisted acid treatment. Influence of the octahedral sheet composition," *Applied Clay Scince*, vol. 196, article 105745, 2020.

[31] M. L. Occelli, "Surface properties and cracking activity of delaminated clay catalysts," *Catalysis Today*, vol. 2, no. 2-3, pp. 339–355, 1988.

[32] J. A. Cecilia, E. Vilarrasa-García, C. L. Cavalcante Jr., D. C. S. Azevedo, F. Franco, and E. Rodríguez-Castellón, "Evaluation of two fibrous clay minerals (sepiolite and palygorskite) for CO_2 capture," *Journal of Environmental Chemical Engineering*, vol. 6, no. 4, pp. 4573–4587, 2018.

[33] M. Thommes, K. Kaneko, A. V. Neimark et al., "Physisorption of gases, with special reference to the evaluation of surface area and pore size distribution (IUPAC technical report)," *Pure and Applied Chemistry*, vol. 87, no. 9-10, pp. 1051–1069, 2015.

[34] B. B. Zviagina, D. K. McCarty, J. Srodón, and V. A. Drits, "Interpretation of infrared spectra of dioctahedral smectites in the region of OH-stretching vibrations," *Clays and Clay Minerals*, vol. 52, no. 4, pp. 399–410, 2004.

[35] J. A. Cecilia, L. Pardo, M. Pozo, E. Bellido, and F. Franco, "Microwave-assisted acid activation of clays composed of 2 : 1 clay minerals: a comparative study," *Minerals*, vol. 8, no. 9, p. 376, 2018.

[36] R. L. Frost, O. B. Locos, H. Ruan, and J. T. Kloprogge, "Near-infrared and mid-infrared spectroscopic study of sepiolites and palygorskites," *Vibrational Spectroscopy*, vol. 27, no. 1, pp. 1–13, 2001.

[37] J. Madejová, "FTIR techniques in clay mineral studies," *Vibrational Spectroscopy*, vol. 31, no. 1, pp. 1–10, 2003.

[38] M. A. Vicente-Rodríguez, M. Suárez, M. A. Bañares-Muñoz, and J. D. López-Suárez, "Comparative FT-IR study of the removal of octahedral cations and structural modifications during acid treatment of several silicates," *Spectrochimica Acta A*, vol. 52, no. 13, pp. 1685–1694, 1996.

[39] J. A. Cecilia, E. Vilarrasa-García, C. García-Sancho et al., "Functionalization of hollow silica microspheres by impregnation or grafted of amine groups for the CO_2 capture," *International Journal of Greenhouse Gas Control*, vol. 52, pp. 344–356, 2016.

[40] M. Eloussaief, A. Sdiri, and M. Benzina, "Modelling the adsorption of mercury onto natural and aluminium pillared clays," *Environmental Science and Pollution Research*, vol. 20, no. 1, pp. 469–479, 2013.

[41] L. R. Sartor and A. C. de Azevedo, "Pilarização de argilas e perspectivas de aplicação e de pesquisa agronômica e ambiental," *Ciencia Rural*, vol. 44, no. 9, pp. 1541–1548, 2014.

[42] Y. Gao, H. Gan, G. Zhang, and Y. Guo, "Visible light assisted Fenton-like degradation of rhodamine B and 4-nitrophenol solutions with a stable poly-hydroxyl-iron/sepiolite catalyst," *Chemical Engineering Journal*, vol. 217, pp. 221–230, 2013.

[43] N. Liu, Y. Y. Song, Y. Qin, X. Gong, and Y. L. Liu, "Chromatic characteristics and anthocyanin compositions of cabernet sauvignon wines: influence of indigenous *Saccharomyces cerevisiae* strains in Ningxia, China," *Food Science and Biotechnology*, vol. 24, no. 6, pp. 1973–1978, 2015.

[44] M. Jafelicci Jr. and L. C. Varanda, "The world of colloids," *Química Nova Na Escola*, vol. 9, pp. 9–13, 1999.

[45] A. B. Das, V. V. Goud, and C. Das, "Adsorption/desorption, diffusion, and thermodynamic properties of anthocyanin from purple rice bran extract on various adsorbents," *Journal of Food Process Engineering*, vol. 41, no. 6, article e12834, 2018.

[46] G. A. F. Hendry and J. D. Houghton, *Natural Food Colorants*, Springer, 1996.

[47] L. C. B. Lima, F. Castro-Silva, E. C. Silva-Filho, M. G. Fonseca, and M. Jaber, "Saponite-anthocyanin pigments: slipping between the sheets," *Microporous and Mesoporous Materials*, vol. 300, article 110148, 2020.

[48] C. Agougui, J. A. Cecilia, H. Saad et al., "Adsorption of Carvone and Limonene from Caraway essential oil onto Tunisian montmorillonite clay for pharmaceutical application," *Scientific Reports*, vol. 12, no. 1, article 19814, 2022.

[49] J. Chandrasekhar, N. Aduja, and K. S. M. S. Raghavarao, "Purification of anthocyanins from jamun (*Syzygium cumini* L.) employing adsorption," *Separation and Purification Technology*, vol. 125, pp. 170–178, 2014.

[50] J. Chandrasekhar, M. C. Madhusudhan, and K. S. M. S. Raghavarao, "Extraction of anthocyanins from red cabbage and purification using adsorption," *Food and Bioproducts Processing*, vol. 90, no. 4, pp. 615–623, 2012.

[51] N. Ahmadiani, R. J. Robbins, T. M. Collins, and M. M. Giusti, "Anthocyanins contents, profiles, and color characteristics of red cabbage extracts from different cultivars and maturity stages," *Journal of Agricultural and Food Chemistry*, vol. 62, no. 30, pp. 7524–7531, 2014.

[52] P. Arapitsas and C. Turner, "Pressurized solvent extraction and monolithic column-HPLC/DAD analysis of anthocyanins in red cabbage," *Talanta*, vol. 74, no. 5, pp. 1218–1223, 2008.

[53] W. Wiczkowski, D. Szawara-Nowak, and J. Topolska, "Red cabbage anthocyanins: profile, isolation, identification, and antioxidant activity," *Food Research International*, vol. 51, no. 1, pp. 303–309, 2013.

[54] P. Arapitsas, P. J. R. Sjöberg, and C. Turner, "Characterisation of anthocyanins in red cabbage using high resolution liquid chromatography coupled with photodiode array detection and electrospray ionization-linear ion trap mass spectrometry," *Food Chemistry*, vol. 109, no. 1, pp. 219–226, 2008.

[55] G. J. McDougall, S. Fyffe, P. Dobson, and D. Stewart, "Anthocyanins from red cabbage-stability to simulated gastrointestinal digestion," *Phytochemistry*, vol. 68, no. 9, pp. 1285–1294, 2007.

[56] J. Sun, Z. Xiao, L. Z. Lin et al., "Profiling polyphenols in five *Brassica* species microgreens by UHPLC-PDA-ESI/HRMS^n," *Journal of Agricultural and Food Chemistry*, vol. 61, no. 46, pp. 10960–10970, 2013.

[57] C. Aza-González and N. Ochoa-Alejo, "Characterization of anthocyanins from fruits of two Mexican chili peppers (*Capsicum Annuum* L.)," *Journal of the Mexican Chemical Society*, vol. 56, no. 2, pp. 149–151, 2017.

[58] T. Shimizu, T. Muroi, T. Ichi, M. Nakamura, and K. Yoshihira, "Analysis of red cabbage colors in commercial foods using high performance liquid chromatography with photodiode array detection-mass spectrophotometry," *Shokuhin Eiseigaku Zasshi*, vol. 38, no. 1, pp. 34–38, 1997.

[59] X. Wu and R. L. Prior, "Identification and characterization of anthocyanins by high-performance liquid chromatography-electrospray ionization-tandem mass spectrometry in common foods in the United States: vegetables, nuts, and grains," *Journal of Agricultural and Food Chemistry*, vol. 53, no. 8, pp. 3101–3113, 2005.

[60] C. S. Charron, B. A. Clevidence, S. J. Britz, and J. A. Novotny, "Effect of dose size on bioavailability of acylated and nonacylated anthocyanins from red cabbage (*Brassica oleracea* L. Var. capitata)," *Journal of Agricultural and Food Chemistry*, vol. 55, no. 13, pp. 5354–5362, 2007.

[61] W. S. W. Ngah and M. A. K. M. Hanafiah, "Biosorption of copper ions from dilute aqueous solutions on base treatedrubber (*Hevea brasiliensis*) leaves powder: kinetics, isotherm, and biosorption mechanisms," *Journal of Environmental Sciences*, vol. 20, no. 10, pp. 1168–1176, 2008.